Article

Deep Transfer Learning for Few-shot SAR Image Classification

Mohammad Rostami[1,2], Soheil Kolouri[1], Eric Eaton[2] and Kuyngnam Kim[1]*

[1] HRL Laboratories; {mrostami,skolouri, kkim}@hrl.com
[2] University of Pennsylvania; eeaton@upenn.seas.edu
* Correspondence: mrostami@hrl.com

Version May 6, 2019 submitted to Preprints

Abstract: Reemergence of deep Neural Networks (CNNs) has lead to high-performance supervised learning algorithms for the Electro-Optical (EO) domain classification and detection problems. This success is possible because generating huge labeled datasets has become possible using modern crowdsourcing labeling platforms such as Amazon Mechanical Turk that recruit ordinary people to label data. Unlike the EO domain, labeling the Synthetic Aperture Radar (SAR) domain data can be a lot more challenging and for various reasons using crowdsourcing platforms is not feasible for labeling the SAR domain data. As a result, training deep networks using supervised learning is more challenging in the SAR domain. In the paper, we present a new framework to train a deep neural network for classifying Synthetic Aperture Radar (SAR) images by eliminating the need for huge labeled dataset. Our idea is based on transferring knowledge from a related EO domain problem, where labeled data is easy to obtain. We transfer knowledge from the EO domain through learning a shared invariant cross-domain embedding space that is also discriminative for classification. To this end, we train two deep encoders that are coupled through their last year to map data points from the EO and the SAR domains to the shared embedding space such that the distance between the distributions of the two domains is minimized in the latent embedding space. We use the Sliced Wasserstein Distance (SWD) to measure and minimize the distance between these two distributions and use a limited number of SAR label data points to match the distributions class-conditionally. As a result of this training procedure, a classifier trained from the embedding space to the label space using mostly the EO data would generalize well on the SAR domain. We provide theoretical analysis to demonstrate why our approach is effective and validate our algorithm on the problem of ship classification in the SAR domain by comparing against several other learning competing approaches.

Keywords: transfer learning; convolutional neural network; electro-optical imaging, synthetic aperture radar (SAR) imaging, optimal transport metric

1. Introduction

Historically and prior to emergence of machine learning, most imaging devices were designed first to generate outputs that are interpretable by humans, mostly natural images. As a result, the dominant visual data that is collected even nowadays is the Electro-Optical (EO) domain data. Digital EO images are generated by a planner grid of sensors that detect and record the magnitude and the color of reflected visible light from the surface of an object in the from of a planner array of pixels. Naturally, most machine learning algorithms that are developed for automation, also process EO domain data as their input. Recently, the area of EO-based machine learning and computer vision has been successful in developing classification and detection algorithms with human-level performance for many applications. In particular, reemergence of neural networks in the form deep Convolutional Neural Networks (CNNs) has been crucial for this success. The major reason for the outperformance of CNNs over many prior classic learning methods is that the time consuming and unclear procedure of feature engineering in classic machine learning and computer vision can be bypassed when CNN are trained. CNNs are able to extract abstract and high-quality discriminative features for a given task automatically in a blind end-to-end supervised training scheme, where CNNs are trained using a huge labeled dataset of images. Since the learned features are task-dependent, often lead to better performance compared to engineered features that are usually defined for broad range of tasks, e.g. wavelet, DFT, SIFT, etc.

 doi:10.20944/preprints201905.0030.v1

Despite wide range of applicability of EO imaging, it is also naturally constrained by limitations of human visual sensory system. In particular, in applications such as continuous environmental monitoring and large-scale surveillance [1], and earth remote sensing [2], continuous imaging at extended time periods and independent of the weather conditions is necessary. EO imaging is not suitable for such applications because imaging during night and cloudy weather is not feasible. In these applications, using other imaging techniques that are designed for imaging beyond the visible spectrum are inevitable. Synthetic Aperture Radar (SAR) imaging is a major technique in this area that is highly effective for remote sensing applications. SAR imaging benefits from radar signals that can propagate in occluded weather and at night. Radar signals are emitted sequentially from a moving antenna and the reflected signals are collected for subsequent signal processing to generate high-resolution images irrespective of the weather conditions and occlusions. While both the EO and the SAR domain images describe the same physical world and often SAR data is represented in a planner array form similar to an EO image, processing EO and SAR data and developing suitable learning algorithms for these domains can be quite different. In particular, replicating the success of CNNs in supervised learning problems of the SAR domain is more challenging. This is because training CNNs is conditioned on the availability of huge labeled datasets to supervise blind end-to-end learning. Until quite recently, generating such datasets was challenging and expensive. Nowadays, labeled datasets for the EO domain tasks are generated using crowdsourcing labeling platforms such as Amazon Mechanical Turk, e.g. ImageNet [3]. In a crowdsourcing platform, a pool of participants with common basic knowledge for labeling EO data points, i.e. natural images, is recruited. These participants need minimal training and in many cases are not even compensated for their time and effort. Unlabeled images are presented to each participant independently and each participant selects a label for each given image. Upon collecting labels from several people from the pool of participants, collected labels are aggregated according to skills and reliability of each participant to increase labeling accuracy [4]. Despite being very effective for generating high quality labeled dataset for EO domains, for various reasons crowdsourcing platforms are not suitable for SAR domains:

- Preparing devices for collecting SAR data, solely for generating training datasets is much more expensive compared to EO datasets [5]. In many cases, EO datasets can even be generated from the Internet using existing images that are taken by commercial cameras. In contrast, SAR imaging devices are not commercial and usually are expensive to operate, e.g. satellites.
- SAR images are often classified data because for many applications the goal is surveillance and target detection. This issue makes access to SAR data heavily regulated and limited to certified people. Even for research purposes, only few datasets are publicly available. This limits the number of participants who can be hired to help with processing and labeling.
- Despite similarities, SAR images are not easy to interpret by an average person. For this reason, labeling SAR images needs trained experts who know how to interpret SAR data. This is in contrast with tasks within the EO domain images, where ordinary people can label images by minimal training and guidance [6]. This challenge makes labeling SAR data more expensive as only professional trained people can perform labeling SAR data.
- Continuous collection of SAR data is common in SAR applications. As a result, distribution of data is likely to be non-stationery. As a result, even a high-quality labeled dataset is generated, the data would become unrepresentative of the current distribution over extended time intervals. This would obligate persistent data labeling to updated a trained model [7].

As a result of the above challenges, generating labeled detests for the SAR domain data is in general difficult. In particular, given the size of most existing SAR datasets, training a CNN leads to overfit models as the number of data points are considerably less than the required sample complexity of training a deep network [8,9]. When the model is overfit, naturally it will not generalize well on test sets. In other words, we face situations in which the amount of accessible labeled SAR data is not sufficient for training a deep neural networks that extract useful features. In the machine learning literature, challenges of learning in this scenario has been investigated within transfer learning [10]. The general idea that we focus on is to transfer knowledge from a secondary domain to reduce the amount labeled data that is necessary to train a model. Building upon prior works in the area of

 doi:10.20944/preprints201905.0030.v1

transfer learning, several recent works have used the idea of knowledge transfer to address challenges of SAR domains [5,7,9,11–13]. The common idea in these works is to transfer knowledge from a secondary related problem, where labeled data is easy and cheap to obtain. For example, the second domain can be a related task in EO domain or a task generated by synthetic data. Following this line of work, our goal in this paper is to tackle challenges of learning in SAR domains when the labeled data is scarce. This particular setting of transfer learning is also called domain adaptation in machine learning literature. In this setting the domain with labeled data scarcity is called the target domain and the domain with sufficient labeled data is called the target domain. We develop a method that benefits from cross-domain knowledge transfer from a related task in EO domains as the source domain to address a task in SAR domains as the target domain. More specifically, we consider a classification task with the same classes in two domains, i.e. SAR and EO. This is a typical situation for many applications, as it is common to use both SAR and EO imaging. We consider a domain adaptation setting, where we have sufficient labeled data points in the source domain, i.e. EO. We also have access to abundant data points in the target domain, i.e. EO, but only few labeled data points are labeled. This setting is called semi-supervised domain adaptation in the machine learning literature [14].

Several approaches have been developed to address the problem of domain adaptation. A common technique for cross-domain knowledge transfer is encode data points of the two related domains in a domain-invariant embedding space such that similarities between the tasks can be identified and captured in the shared space. As a result, knowledge can be transferred across the domains in the embedding space through correspondences that are captured between the domains in the shared space. The key challenge is how to find such an embedding space. In this paper, we model the shared embedding space as the output space of deep encoders. we couple two deep encoders to map the data points from the EO and the SAR domains into a shared embedding space as their outputs such that both domains would have similar distributions in this space. If both domains have similar class-conditional probability distributions in the embedding space, then if we train a classifier network using only the source-domain labeled data points from the shared embedding to the label space, it will also generalize well on the target domain test data points [15]. This goal can be achieved by training the deep encoders as two deterministic functions using training data such that the empirical distribution discrepancy between the two domains is minimized in the shared output of the deep encoders with respect to some probability distribution metric[16,17].

Our contribution is to propose a novel semi-supervised domain adaptation algorithm to transfer knowledge from the EO domain to the SAR domain using the above explained procedure. We train the encoder networks by using the Sliced-Wasserstein Distance (SWD) [18] to measure and then minimize the discrepancy between the source and the target domain distributions. There are two majors reasons for using SWD. First, SWD is an effective metric for the space of probability distributions that can be computed efficiently. Second, SWD is non-zero even for two probability distributions with non-overlapping supports. As a result, it has non-vanishing gradients and first-order gradient-based optimization algorithms can be used to solve optimization problems involving SWD terms [15,19]. This is important as most optimization problems for training deep neural networks are solved using gradient-based methods, e.g. stochastic gradient descent (SGD). The above procedure might not succeed because while the distance between distributions may be minimized, they may not be aligned class-conditionally. We use the few accessible labeled data points in the SAR domain to align both distributions class-conditionally to tackle the class matching challenge [20]. We demonstrate theoretically why our approach is able to train a classifier with generalizability on the target SAR domain. We also provide experimental results to validate our approach in the area of maritime domain awareness, where the goal is to understand activities that could impact the safety and the environment. Our results demonstrate our approach is effective and leads to state-of-the-art performance.

2. Related Work

Recently, several prior works have addressed classification in SAR domain in label-scarce regime. Huang et al. [7] us an unsupervised learning approach to generate discriminative features. Given that generating unlabeled SAR data is easier, their idea is to train a deep autoencoder using a large pool of unlabeled SAR data. Upon training the autoencoder, features extracted in the middle-layer of the autoencoder capture difference across

 doi:10.20944/preprints201905.0030.v1

different classes and can be used for classification. For example, The trained encoder sub-network of the autoencoder can be concatenated with a classifier network and both would be fine-tuned using the labeled portion of data to map the data points to the label space. In other words, the deep encoder is used as a task-dependent feature extractor. Hansen et al. [5] proposed to transfer knowledge using synthetic SAR images which are easy to generate and are similar to real images. Their idea is to to generate a simulated dataset for a given SAR problem based on simulated object radar reflectivity. Upon generating the synthetic labeled dataset, it can be used to pretrain a CNN network prior to presenting the real data. The pretrained CNN then can be used an initialization for the real SAR domain problem. Due to the pretraining stage and similarities between the synthetic and the read data, the model can be thought of a better initial point and hence fine-tuned using fewer real labeled data points. Zhang et al. [11] propose to transfer knowledge from a secondary source SAR task, where labeled data is available. Similarly, a CNN network can be pretrained on the task with labeled data and then fine-tuned on the target task. Lang et al. [13] use automatic identification system (AIS) as the secondary domain for knowledge transfer. AIS is a tracking system for monitoring movement of ships that can provide labeling information. Shang et al. [9] amend a CNN with an information recorder. The recorder is used to store spatial features of labeled samples and the recorded features are used to predict labels of unlabeled data points based on spatial similarity to increase the number of labeled samples. Finally, Weng et al. [12] use an approach more similar to our framework. Their proposal is to transfer knowledge from EO domain using VGGNet as a feature extractor in the learning pipeline, which itself has been pretrained on a large EO dataset. Despite being effective, the common idea of these past works is mostly using a deep network that is pretrained using a secondary source of knowledge, which is then fine-tuned using few labeled data points on the target SAR task. Hence, knowledge transfer occurs as a result of selecting a better initial point for the optimization problem using the secondary source. We follow a different approach by recasting the problem as a domain adaptation (DA) problem [17], where the goal is to adapt a model trained on the source domain to generalize well in the target domain. Our contribution is to demonstrate how to transfer knowledge from EO imaging domain in order to train a deep network for the SAR domain. The idea is to use a related EO domain problem with abundant labeled data when training a deep network on a related EO problem with abundant labeled data and simultaneously adapt the model considering that only few labeled SAR data points are accessible. In our training scheme, we enforce the distributions of both domains to become similar within a mid-layer of the deep network.

Domain adaptation has been investigated in the computer vision literature for a broad range of application for the EO domain problems. The goal in domain adaptation is to train a model on a source data distribution with sufficient labeled data such that it generalizes well on a different, but related target data distribution, where labeling data is challenging. Despite being different, the common idea of DA approaches is to preprocess data from both domains or at least the target domain such that the distributions of both domains become similar after preprocessing. Doing, a classifier which is trained using the source data, can also be used on the target domain due to post-processing similar distributions. In this paper, we consider that two deep convolutional neural networks preprocess data to enforce both EO and SAR domains data to have similar probability distributions. To this end, we couple two deep encoder sub-networks with a shared output space to model the embedding space. This space can be considered as an intermediate embedding space between the input space from each domain and the label space of a classifier network that is shared between the two domains. These deep encoders are trained such that the discrepancy between the source and the target domain distributions is minimized in the shared embedding space, while overall classification is supervised mostly via the EO domain labeled data. This procedure can be done via adversarial learning [21], where the distributions are matched indirectly. We can also formulated an optimization problem with probability matching objective to match the distributions directly [22]. We use the latter apporach for in our approach.

In order to minimize the distance between two probability distributions, we need to select a measure of distance between two empirical distributions and then minimize it using the training data from both domains. Early works in domain adaptation used the Maximum Mean Discrepancy (MMD) metric for this purpose [17]. MMD measures the distance between two distribution as the Euclidean distance between their means. However, MMD might not be an accurate measure when the distributions are multi-modal. while other well-studied discrepancy measures such as KL-divergence and Jensen-Shannon divergence have been used for a broad range

Preprints (www.preprints.org) | NOT PEER-REVIEWED | Posted: 6 May 2019 doi:10.20944/preprints201905.0030.v1

of domain adaptation problems [23], these measures have vanishing gradients when the distributions have non-overlapping support. This situation can occur in initial iterations of training when the distributions are still distant. This problem makes KL-divergence and Jensen-Shannon divergence inappropriate for deep learning as deep networks are trained using gradient-based first-order optimization techniques which require gradient information [24]. For this reason, recent works the Wasserstein Distance (WD) metric [16] has gained interest as an objective function to match distributions in the deep learning community. WD has non-vanishing gradient but it does not have a closed-form definition and is defined as a linear programming (LP) problem. Solving the LP problem can be computationally expensive for high-dimensional distributions. For this reason, there is also interest to compute or approximate WD to reduce the computational burden. In this paper, we use the Sliced Wasserstein Distance (SWD) to circumvent this challenge. SWD approximates WD as sum of multiple Wasserstein distances of one-dimensional distributions which possess a closed-form solution and can be computed efficiently [18,24–26].

3. Problem Formulation and Rationale

Let $\mathcal{X}^{(t)} \subset \mathbb{R}^d$ denote the domain space of SAR data. Consider a multiclass SAR classification problem with k classes in this domain, where i.i.d data pairs are drawn from the joint probability distribution, i.e. $(\boldsymbol{x}_i^t, \boldsymbol{y}_i^t) \sim q_T(\boldsymbol{x}, \boldsymbol{y})$ which has the marginal distribution $p_T(\boldsymbol{x})$ over $\mathcal{X}^{(t)}$. Here, a label $\boldsymbol{y}_i^t \in \mathcal{Y}$ identifies the class membership of the vectorized SAR image $\boldsymbol{x}_t^i$ to one of the k classes. We have access to $M \gg 1$ unlabeled images $\mathcal{D}_\mathcal{T} = (\boldsymbol{X}_\mathcal{T} = [\boldsymbol{x}_1^t, \ldots, \boldsymbol{x}_M^t]) \in \mathbb{R}^{d \times M}$ in this target domain. Additionally, we have have access to O labeled images $\mathcal{D'}_\mathcal{T} = (\boldsymbol{X'_\mathcal{T}}, \boldsymbol{Y'_\mathcal{T}})$, where $\boldsymbol{X'_\mathcal{S}} = [\boldsymbol{x}_1^{'t}, \ldots, \boldsymbol{x}_O^{'t}] \in \mathbb{R}^{d \times O}$ and $\boldsymbol{Y'_\mathcal{S}} = [\boldsymbol{y}_1^{'t}, \ldots, \boldsymbol{y}_O^{'t}] \subset \mathbb{R}^{k \times O}$ contains the corresponding one-hot labels. The goal is to train a parameterized classifier $f_\theta : \mathbb{R}^d \to \mathcal{Y} \subset \mathbb{R}^k$, i.e. a deep neural network with weight parameters θ, on this domain. Given that we have access to only few labeled data points and considering model complexity of deep neural networks, training the deep network such that it generalizes well using solely the SAR labeled data is not feasible as training would lead to overfitting on the few labeled data points such that the trained network would generalize poorly on test data points.

To tackle the problem of label scarcity, we consider a domain adaptation scenario. We assume that a related source EO domain problem exists, were we have access to sufficient labeled data points such that training a generalizable model is feasible. Let $\mathcal{X}^{(s)} \subset \mathbb{R}^{d'}$ denote the EO domain $\mathcal{D}_\mathcal{S} = (\boldsymbol{X}_\mathcal{S}, \boldsymbol{Y}_\mathcal{S})$ denote the dataset in the EO domain, with $\boldsymbol{X}_\mathcal{S} \in \mathcal{X} \subset \mathbb{R}^{d' \times N}$ and $\boldsymbol{Y}_\mathcal{S} \in \mathcal{Y} \subset \mathbb{R}^{k \times N}$ ($N \gg 1$). Note that since we consider the same cross-domain classes, we are considering the same classification problem in two domains. This cross-domain similarity is necessary for making knowledge transfer feasible. In other words, we have a classification problem with bi-modal data but there is no point-wise correspondence across the data modals and in most data points in one of them are unlabeled. We assume the source samples are drawn i.i.d. from the source joint probability distribution $q_\mathcal{S}(\boldsymbol{x}, \boldsymbol{y})$, which has the marginal distribution p_S. Note that despite similarities between the domains, the marginal distributions of the domains are different. Given that extensive research and investigation has been done in EO domains, we hypothesize that finding such a labeled dataset is likely feasible or labeling such an EO data is easier than labeling more SAR data points. Our goal is to use the similarity between the EO and the SAR domains and benefit from the unlabeled SAR data to train a model for classifying SAR images using the knowledge that can be learned from the EO domain.

Since we have access to sufficient labeled source data, training a parametric classifier for the source domain is a straightforward supervised learning problem. Usually, we solve for an optimal parameter to select the best the best model form the family of parametric functions f_θ. We can solve for an optimal parameter by minimizing the average empirical risk on the training labeled data points, i.e. empirical risk minimization (ERM):

$$\hat{\theta} = \arg\min_\theta \hat{e}_\theta = \arg\min_\theta \frac{1}{N} \sum_{i=1}^{N} \mathcal{L}(f_\theta(\boldsymbol{x}_i^s), \boldsymbol{y}_i^s) \ , \tag{1}$$

where $\mathcal{L}$ is a proper loss function (e.g., cross entropy loss). Given enough training data points, the empirical risk is a suitable surrogate for the real risk function:

$$e = \mathbb{E}_{(\boldsymbol{x},\boldsymbol{y}) \sim p_\mathcal{S}(\boldsymbol{x},\boldsymbol{y})}(\mathcal{L}(f_\theta(\boldsymbol{x}), \boldsymbol{y})) \ , \tag{2}$$

Preprints (www.preprints.org) | NOT PEER-REVIEWED | Posted: 6 May 2019 doi:10.20944/preprints201905.0030.v1

which is the objective function for Bayes optimal inference. This means that the learned classifier would generalize well on data points if they are drawn from p_S. A naive approach to transfer knowledge from the EO domain to the SAR domain is to use the classifier that is trained on the EO domain directly in the target domain. However, since distribution discrepancy exists between the two domains, i.e. $p_S \neq p_T$, the trained classifier on the source domain $f_{\hat{\theta}}$, might not generalize well on the target domain. Therefore, there is a need for adapting the training procedure for $f_{\hat{\theta}}$. The simplest approach which has been used in most prior works is to fine-tune the EO classifier using the few labeled target data points to employ the model in the target domain. This approach would add the constraint of $d = d'$ as the same input space is required to use the same network across the domains. Usually it is easy to use image interpolation to enforce this condition, but information maybe lost after interpolation. We want to use a more principled approach and remove the condition of $d = d'$. More importantly, when fine-tuning is used, unlabeled data is not used. We want to take advantage and benefit from the unlabeled SAR data points which are accessible and provide additional information about the SAR domain marginal distribution.

Figure 1 presents a block diagram visualization of our framework. In the figure, we have visualized images from two related real world SAR and EO datasets that we have used in the experimental section of the paper. The task is classify Ship images. Notice that SAR images are confusing for the untrained human eye, while EO ship/no-ship images can be distinguished by minimal inspection. This suggests that as we discussed before, SAR labeling is more challenging and requires expertise. In our approach, we consider the EO deep network $f_\theta(\cdot)$ to be formed by a feature extractor $\phi_v(\cdot)$, i.e. convolutional layers of the network, which is followed by a classifier sub-network $h_w(\cdot)$, i.e. fully connected layers of the network, that inputs the extracted feature and maps them to the label space. Here, w and v denote the corresponding learnable parameters for these sub-networks, i.e. $\theta = (w, v)$. This decomposition is synthetic but helps to understand our approach. In other words, the feature extractor sub-network $\phi_v : \mathcal{X} \to \mathcal{Z}$ maps the data points into a discriminative embedding space $\mathcal{Z} \subset \mathbb{R}^f$, where classification can be done easily by the classifier sub-network $h_w : \mathcal{Z} \to \mathcal{Y}$. The success of deep learning stems from optimal feature extraction which converts the data distribution into a multimodal distribution which makes class separation feasible. Following the above, we can consider a second encoder network $\psi_u(\cdot) : \mathbb{R}^d \to \mathbb{R}^f$, which maps the SAR data points to the same target embedding space at its output. The idea that we want to explore is based on training ϕ_v and ψ_u such that the discrepancy between the source distribution $p_{\mathcal{S}}(\phi(\boldsymbol{x}))$ and target distribution $p_{\mathcal{T}}(\phi(\boldsymbol{x}))$ is minimized in the shared embedding space, modeled as the shared output space of these two encoders. As a result of matching the two distributions, the embedding space becomes invariant with respect to the domain. In other words, data points from the two domains become indistinguishable in the embedding space, e.g. data points belonging to the same class are mapped into the same geometric cluster in the shared embedding space as depicted in Figure 1. Consequently, even if we train the classifier sub-network using solely the source labeled data points, it will still generalize well when target data points are used for testing. The key question is how to train the encoder sub-networks such that the embedding space becomes invariant. We need to adapt the standard supervised learning in Eq. (1) by adding additional terms that enforce cross-domain distribution matching.

4. Proposed Solution

In our solution, the encoder sub-networks need to be learned such that the extracted features in the encoder output are discriminative. Only then, the classes become separable for the classifier sub-network (see Figure 1). This is a direct result of supervised learning for EO encoder. Additionally, the encoders should mix the SAR and the EO domains such that the embedding becomes domain-invariant. As a result, the SAR encoder is indirectly enforced to be discriminative for the SAR domain. We enforce the embedding to be domain-invariant

Preprints (www.preprints.org) | NOT PEER-REVIEWED | Posted: 6 May 2019 doi:10.20944/preprints201905.0030.v1

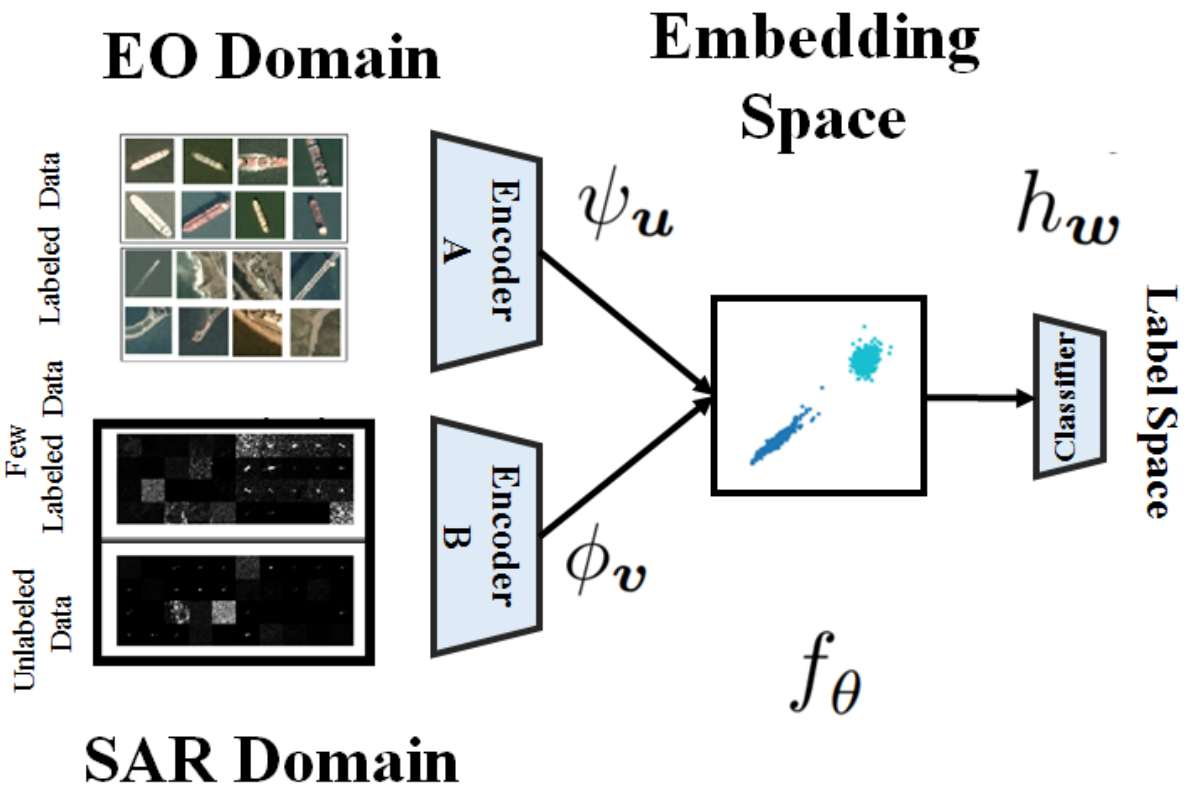

Figure 1. Block diagram architecture of the proposed framework for transferring knowledge from the EO to the SAR domain.

by minimizing the discrepancy between the distributions of both domains in the embedding space. Following the above, we can formulate the following optimization problem for computing the optimal values for $\boldsymbol{v}, \boldsymbol{u}$ and $\boldsymbol{w}$:

$$\begin{aligned}\min_{v,u,w} \frac{1}{N}\sum_{i=1}^{N}\mathcal{L}\big(h_w(\phi_v(\boldsymbol{x}_i^s)),\boldsymbol{y}_i^s\big)+\frac{1}{O}\sum_{i=1}^{O}\mathcal{L}\big(h_w(\psi_u(\boldsymbol{x}_i^{'t})),\boldsymbol{y}_i^{'t}\big)\\ +\lambda D\big(\phi_v(p_{\mathcal{S}}(\boldsymbol{X}_{\mathcal{S}})),\psi_u(p_{\mathcal{T}}(\boldsymbol{X}_{\mathcal{T}}))\big)+\eta\sum_{j=1}^{k}D\big(\phi_v(p_{\mathcal{S}}(\boldsymbol{X}_{\mathcal{S}})|C_j),\psi_u(p_{\mathcal{T}}(\boldsymbol{X}'_{\mathcal{T}})|C_j)\big)\ ,\end{aligned} \tag{3}$$

where $D(\cdot,\cdot)$ is a discrepancy measure between the probabilities and λ and η are trade-off parameters. The first two terms in Eq. (3) are standard empirical risks for classifying the EO and SAR labeled data points, respectively. The third term is the cross-domain unconditional probability matching loss. We match the unconditional distributions as the SAR data is mostly unlabeled. The matching loss is computed using all available data points from both domains to learn the learnable parameters of encoder sub-networks and the classifier sub-network is simultaneously learned using the labeled data from both domains. Finally, the last term is Eq. (3) is added to enforce semantic consistency between the two domains by match the distributions class-conditionally. This term is important for knowledge transfer. To clarify this point, note that the domains might be aligned such that their marginal distributions $\phi(p_{\mathcal{S}}(\boldsymbol{X}_{\mathcal{S}}))$ and $\psi(p_{\mathcal{T}}(\boldsymbol{X}_{\mathcal{T}}))$ have minimal discrepancy, while the distance between $\phi(q_{\mathcal{S}}(\cdot,\cdot))$ and $\psi(q_{\mathcal{T}}(\cdot,\cdot))$ is not minimized. This means that the classes may not have been aligned correctly, e.g. images belonging to a class in the target domain may be matched to a wrong class in the source domain or, even worse, images from multiple classes in the target domain may be matched to the cluster of another class of the source domain. In such cases, the classifier will not generalize well on the target domain as it has been trained to be consistent with spatial arrangement of the source domain in the embedding space. This means that if we merely minimize the distance between $\phi(p_{\mathcal{S}}(\boldsymbol{X}_{\mathcal{S}}))$ and $\psi(p_{\mathcal{T}}(\boldsymbol{X}_{\mathcal{T}}))$, the shared embedding space might not be a consistently discriminative space for both domains domain in terms of classes. The challenge

Preprints (www.preprints.org) | NOT PEER-REVIEWED | Posted: 6 May 2019 doi:10.20944/preprints201905.0030.v1

Algorithm 1 FCS (L, η, λ)

Input: data

$\mathcal{D}_{\mathcal{S}} = (\boldsymbol{X}_{\mathcal{S}}, \boldsymbol{Y}_{\mathcal{S}}); \mathcal{D}_{\mathcal{T}} = (\boldsymbol{X}_{\mathcal{T}},, \boldsymbol{Y}_{\mathcal{T}}), \mathcal{D}'_{\mathcal{T}} = (\boldsymbol{X}'_{\mathcal{T}}),$

Pre-training: initialization

$\hat{\theta}_0 = (\boldsymbol{w}_0, \boldsymbol{v}_0) = \arg\min_\theta 1/N \sum_{i=1}^{N} \mathcal{L}(f_\theta(\boldsymbol{x}_i^s), \boldsymbol{y}_i^s)$

for $itr = 1, \ldots, ITR$ **do**

Update encoder parameters using:

$\hat{\boldsymbol{v}}, \hat{\boldsymbol{u}} = \lambda D(\phi_{\boldsymbol{v}}(p_{\mathcal{S}}(\boldsymbol{X}_{\mathcal{S}})), \psi_{\boldsymbol{u}}(p_{\mathcal{T}}(\boldsymbol{X}_{\mathcal{T}})))$

$+\eta \sum_j D(\phi_{\boldsymbol{v}}(p_{\mathcal{S}}(\boldsymbol{X}_{\mathcal{S}})|C_j), \psi_{\boldsymbol{v}}(p_{\mathcal{SL}}(\boldsymbol{X}'_{\mathcal{T}})|C_j))$

Update entire parameters:

$\hat{\boldsymbol{v}}, \hat{\boldsymbol{u}}, \hat{\boldsymbol{w}} = \arg\min_{\boldsymbol{w},\boldsymbol{v},\boldsymbol{u}} 1/N \sum_{i=1}^{N} \mathcal{L}\big(h_{\boldsymbol{w}}(\phi_{\boldsymbol{v}}(\boldsymbol{x}_i^s)), \boldsymbol{y}_i^s\big)$

$+1/O \sum_{i=1}^{O} \mathcal{L}\big(h_{\boldsymbol{w}}(\psi_{\boldsymbol{u}}(\boldsymbol{x}_i'^t)), \boldsymbol{y}_i'^t\big)$

end for

of class-matching is a known problem in domain adaptation and several approaches have been developed to address this challenge [27]. In our framework, the few labeled data points in the target SAR domain can be used to match the classes consistently across both domains. We use these data points to compute the fourth term in Eq. (3). This term is added to match class-conditional probabilities of both domains in the embedding space, i.e. $\phi(p_{\mathcal{S}}(\boldsymbol{x}_{\mathcal{S}})|C_j) \approx \psi(p_{\mathcal{T}}(\boldsymbol{x}|C_j)$, where C_j denotes a particular class.

The remaining key question is selecting a proper metric to compute $D(\cdot,\cdot)$ in the last two terms of Eq 1. KL-divergence and Jensen-Shannon divergence have been used extensively to measure closeness of probability distributions as maximizing the log-likelihood is equivalent to minimizing the KL-divergence between two distributions but as we discussed since stochastic gradient descend is the standard technique to solve the optimization problem in Eq 1, KL-divergence and Jensen-Shannon divergence are not suitable for deep learning applications. This is a major reason for success of adversarial learning as the discrepancy beteen two distributions is minimized indirectly without requiring minimizing a metric [21]. Additionally, the distributions $\phi(p_{\mathcal{S}}(\boldsymbol{x})$ and $\psi(p_{\mathcal{T}}(\boldsymbol{x})$ are unknown and we can rely only on observed samples from these distributions. Therefore, we should be able to compute the discrepancy measure, $D(\cdot,\cdot)$ using only the drawn samples. Optimal transport [16] is a suitable metric to deal with the above issues. For this reason, it has been found to be an effective metric and has been used extensively in deep learning literature recently [15,22,28,29]. Wasserstein Distance is defined in terms of an optimization problem which can be computationally expensive to solve for high-dimensional data. For this reason, efficient approximations and variants for it has been an active research area. In this paper, we use the Sliced Wasserstein Distance (SWD) [30] which is a good approximate of optimal transport [19] and additionally can be computed more efficiently.

Although the Wasserstein distance is defined as the solution to a linear programming problem, but for the case of one-dimensional probability distributions, this problem has a closed form solution which can be computed efficiently. The solution is equal to the ℓ_p-distance between the inverse of the cumulative distribution functions of the two distributions. SWD has been proposed to benefit from this property to simplify computation of the Wasserstein distance. The idea is to decompose a d-dimensional distributions into one-dimension marginal distributions by projecting the distribution along all possible hyperplanes that cover the space. This process is called slicing the high-dimensional distributions. For a distribution $p_{\mathcal{S}}$, a one-dimensional slice of the distribution along the projection direction γ is defined as:

$$\mathcal{R}p_{\mathcal{S}}(t;\gamma) = \int_{\mathcal{S}} p_{\mathcal{S}}(\boldsymbol{x})\delta(t - \langle\gamma, \boldsymbol{x}\rangle)d\boldsymbol{x} \ , \tag{4}$$

where $\delta(\cdot)$ denotes the Kronecker delta function, $\langle\cdot,\cdot\rangle$ denotes the vector dot product, and $\mathbb{S}^{d-1}$ is the d-dimensional unit sphere. We can see that $\mathcal{R}p_{\mathcal{S}}(\cdot;\gamma)$ is computed via integrating $p_{\mathcal{S}}$ over the hyperplanes which are orthogonal to the projection directions γ that cover the space.

Preprints (www.preprints.org) | NOT PEER-REVIEWED | Posted: 6 May 2019 doi:10.20944/preprints201905.0030.v1

The SWD is computed by integrating the Wasserstein distance between sliced distributions over all γ:

$$SW(p_{\mathcal{S}}, p_{\mathcal{T}}) = \int_{\mathbb{S}^{d-1}} W(\mathcal{R}p_{\mathcal{S}}(\cdot;\gamma), \mathcal{R}p_{\mathcal{T}}(\cdot;\gamma))d\gamma \ , \tag{5}$$

where $W(\cdot,\cdot)$ denotes the Wasserstein distance. Computing the above integral directly, is computationally expensive. But, we can approximate the integral in Eq. (5) using a Monte Carlo style integration by choosing L number of random projection directions γ and after computing the Wasserstein distance, average along the random directions. Doing so, our approximation is proportional to $O(\frac{1}{\sqrt{L}})$ and hence we can get a good approximation using Monte Carlo approximation.

In our problem, since we have access only to samples from the two source and target distributions, so we approximate the one-dimensional Wasserstein distance as the ℓ_p-distance between the sorted samples, as the empirical commutative probability distributions. Following the above procedure, the SWD between f-dimensional samples $\{\phi(\mathbf{x}_i^{\mathcal{S}}) \in \mathbb{R}^f \sim p_{\mathcal{S}}\}_{i=1}^M$ and $\{\phi(\mathbf{x}_i^{\mathcal{T}}) \in \mathbb{R}^f \sim p_{\mathcal{T}}\}_{j=1}^M$ can be approximated as the following sum:

$$SW^2(p_{\mathcal{S}}, p_{\mathcal{T}}) \approx \frac{1}{L}\sum_{l=1}^{L}\sum_{i=1}^{M} |\langle \gamma_l, \phi(\mathbf{x}^{\mathcal{S}}_{s_l[i]})\rangle - \langle \gamma_l, \phi(\mathbf{x}^{\mathcal{T}}_{t_l[i]})\rangle|^2 \ , \tag{6}$$

where $\gamma_l \in \mathbb{S}^{f-1}$ is uniformly drawn random sample from the unit f-dimensional ball $\mathbb{S}^{f-1}$, and $s_l[i]$ and $t_l[i]$ are the sorted indices of $\{\gamma_l \cdot \phi(\mathbf{x}_i)\}_{i=1}^M$ for source and target domains, respectively. We utilize the SWD as the discrepancy measure between the probability distributions to match them in the embedding space. Our proposed algorithm for few-shot SAR image classification (FSC) using cross-domain knowledge transfer is summarized in Algorithm 1. Note that we have added a pretraining step which trains the EO encoder and the shared classifier sub-network solely on the EO domain, to be used a better initial point for the next steps of the optimization. Since our problem is non-convex, a good initial point is critical for finding a good local solution.

5. Theoretical Analysis

In order to demonstrate that our approach is effective, we show that transferring knowledge from the EO domain can reduce the real task on the SAR domain. Our analysis is based on broad results for domain adaptation and is not limited to the case of EO-to-SAR transfer. We rely on theoretical results that demonstrate the true target risk for a model that is trained on a source domain is upperbounded by the discrepancy between distributions of the source and the target domains. Various works have used different discrepancy measures for this analysis, but we rely on a version for which optimal transport is used as the discrepancy measure [15]. We use this result and demonstrate why training procedure of our algorithm can train models that generalize well on the target domain.

Redko et al. [15] analyze a standard domain adaptation framework, where the same shared classifier $h_w(\cdot)$ is used on both the source and the target domain. This is analogous to our formulation as the classifier network is shared across the domains in our framework. They use a standard PAC-learning formalism. Accordingly, the hypothesis class is the set of all model $h_w(\cdot)$ that are parameterized by θ and the goal is to select the best model from the hypothesis class. For any member of this hypothesis class, we denote the true risk on the source domain by $e_{\mathcal{S}}$ and the true risk on the target domain with $e_{\mathcal{T}}$. Analogously, $\hat{\mu}_{\mathcal{S}} = \frac{1}{N}\sum_{n=1}^{N}\delta(\boldsymbol{x}_n^s)$ denote the empirical marginal source distribution, which is computed using the training samples and $\hat{\mu}_{\mathcal{T}} = \frac{1}{M}\sum_{m=1}^{M}\delta(\boldsymbol{x}_m^t)$ similarly denotes the empirical target distribution. In this setting, conditioned on availability of labeled data on both domains, we can train a model jointly on both distributions. Let h_{w^*} denote such a ideal model that minimizes the combined source and target risks $e_{\mathcal{C}}(w^*)$:

$$w^* = \arg\min_w e_{\mathcal{C}}(w) = \arg\min_w \{e_{\mathcal{S}} + e_{\mathcal{T}}\} \ . \tag{7}$$

If the hypothesis class is complex enough and given sufficient labeled target domain data, the joint model can be trained such that it generalizes well on both domains. This term is to measure an upperbound for the target risk. Redko et al. [22] proved the following theorem in standard domain adaptation which provides an upper-bound on the target domain risk given the source domain risk and the joint combined risk.

Preprints (www.preprints.org) | NOT PEER-REVIEWED | Posted: 6 May 2019 doi:10.20944/preprints201905.0030.v1

Theorem 5.1. *[15] Under the assumptions described above for UDA, then for any $d' > d$ and $\zeta < \sqrt{2}$, there exists a constant number N_0 depending on d' such that for any $\xi > 0$ and $\min(N, M) \geq \max(\xi^{-(d'+2),1})$ with probability at least $1 - \xi$ for all h_w, the following holds:*

$$e_{\mathcal{T}} \leq e_{\mathcal{S}} + W(\hat{\mu}_{\mathcal{T}}, \hat{\mu}_{\mathcal{S}}) + e_{\mathcal{C}}(w^*) + \sqrt{(2\log(\frac{1}{\xi})/\zeta)}(\sqrt{\frac{1}{N}} + \sqrt{\frac{1}{M}}). \tag{8}$$

Note that although we use SWD in our approach, but it has been theoretically demonstrated that SWD is a good approximation for computing the Wasserstein distance [31]:

$$SW_2(p_X, p_Y) \leq W_2(p_X, p_Y) \leq \alpha SW_2^{\beta}(p_X, p_Y) \tag{9}$$

where α is a constant and $\beta = (2(d+1))^{-1}$ (see [32] for more details). For this reasons, minimizing the SWD metric enforces minimizing WD.

The proof for Theorem 5.1 is based on the fact that the Wasserstein distance between a distribution μ and its empirical approximation $\hat{\mu}$ using N identically drawn samples can be be made small as desired given existence of large enough number of samples N [15]. More specifically, in the setting of Theorem 5.1, we have:

$$W(\mu, \hat{\mu}) \leq \sqrt{(2\log(\frac{1}{\xi})/\zeta)}\sqrt{\frac{1}{N}} \ . \tag{10}$$

We need this property for our analysis. Additionally, we consider bounded loss functions and consider the loss function is normalized by its upperbound. Interested reader may refer to Redko et al. for more details of derivation of this property [15].

Inspection of the Theorem 5.1 might lead to the conclusion that if we minimize the Wasserstein distance between the source and the target marginal distributions in the input space of the model, then we can improve generalization error on the target domain as doing so the upperbound on the target true risk will become tighter in Eq. (8). Thus, performance on the target domain will be close to the performance on the source domain which is small for a model with good performance on the source domain. But there is no guarantee that if we solely minimize the distance between the marginal distributions, then a joint optimal model h_{w^*} with small joint error would exist. This is important as the third term in the right hand side of Eq. (8) would become small only if such a joint model exists. This conclusion might seem unintuitive, but consider a binary classification problem. This situation can happen if the wrong classes are matched across the two domains. In other words, we may minimize the distance between the marginal distribution, but data points from each class are matched to the opposite class in the other domain. Then training a joint model that performs well for both classes is not possible. Hence, we need to minimize the Wasserstein distance between the marginal distributions such that analogous classes across the domains align in the embedding space in order to consider all terms in Theorem 5.1. In our algorithm, the few target labeled data points are used to minimize the joint order. Building upon the above result, we provide the following lemma for our algorithm.

Lemma 5.1. *Consider we use the target dataset labeled data in a semi-supervised domain adaptation scenario in the algorithm 1. Then, the following inequality for the target true risk holds:*

$$e_{\mathcal{T}} \leq e_{\mathcal{S}} + W(\hat{\mu}_{\mathcal{S}}, \hat{\mu}_{\mathcal{PL}}) + \hat{e}_{\mathcal{C}'}(w^*) + \sqrt{(2\log(\frac{1}{\xi})/\zeta)}(2\sqrt{\frac{1}{N}} + \sqrt{\frac{1}{M}} + \sqrt{\frac{1}{O}}) \ , \tag{11}$$

where $\hat{e}_{\mathcal{C}'}(w^*)$ denote the empirical risk of the optimally joint model h_{w^*} on both the source domain and the target labeled data points.

Proof: We use μ_{TS} to denote the combined distribution of both domains. The model parameter w^* is trained for this distribution using ERM on the joint empirical distribution: $\hat{\mu}_{TS} = \frac{1}{N}\sum_{n=1}^{N}\delta(\boldsymbol{x}_n^s) + \frac{1}{O}\sum_{n=1}^{O}\delta(\boldsymbol{x}_n^{'t})$. We

Preprints (www.preprints.org) | NOT PEER-REVIEWED | Posted: 6 May 2019 doi:10.20944/preprints201905.0030.v1

note that given this definition and considering the corresponding joint empirical distribution, $p_{ST}(\boldsymbol{x}, \boldsymbol{y})$, it is easy to show that $e_{\hat{TS}} = \hat{e}_{\mathcal{C}'}(w^*)$. In other words, we can denote the empirical risk for the model as the true risk for the empirical distribution.

$$\begin{aligned} e_{\mathcal{C}'}(w^*) = \hat{e}_{\mathcal{C}'}(w^*) + \left(e_{\mathcal{C}'}(w^*) - \hat{e}_{\mathcal{C}'}(w^*)\right) &\leq \hat{e}_{\mathcal{C}'}(w^*) + W(\mu_{TS}, \hat{\mu}_{TS}) \\ &\leq \hat{e}_{\mathcal{C}'}(w^*)) + \sqrt{(2\log(\frac{1}{\xi})/\zeta)}\left(\sqrt{\frac{1}{N}} + \sqrt{\frac{1}{O}}\right) . \end{aligned} \tag{12}$$

We have used the definition of expectation and the Cauchy-Schwarz inequality to deduce the first inequality in Eq. (12). We have also used the above mentioned property of the Wasserstein distance in Eq. (10) to deduce the second inequality. Now combining Eq. (12) and Eq. (8) completes our proof.

According to Lemma 5.1, the most important samples are the few labeled samples in the target domain as the corresponding term is dominant among the constant terms in Eq. (11) (note $O \ll M$ and $O \ll N$). As we argued, these samples are important to circumvent the class matching challence across the two domains.

6. Experimental Validation

In section we validate our approach empirically. We demonstrated effectiveness of our method in the area of maritime domain awareness on SAR ship detection problem.

6.1. Ship detection in SAR domain

We tested our approach in the binary problem of ship detection using SAR imaging [6]. This problem arises within maritime domain awareness (MDA) where the goal is monitoring ocean continually to decipher maritime activities that could impact the safety of the environment. Detecting ships is important in this application as the majority of important activities that are important is related to ships and their movements. Traditionally, planes and patrol vessels are used for monitoring, but these methods are effective only for limited areas and time periods. As the regulated area expands and monitoring period becomes extended, these methods become time consuming and inefficient. To circumvent these limitations, it is essential to make this process automatic such that it requires minimal human intervention. To reach this goal, satellite imaging is highly effective because large areas of ocean can be monitored. The generated satellite images can be processed using image processing and machine learning techniques automatically. Satellite imaging has been performed using satellite with both EO and SAR imaging devices. However, only SAR imaging allows continual monitoring during broad range of weather conditions and during night. This property is important because illegal activities likely to happen during night and during occluded weather, human errors are likely to occur. For these reasons, SAR imaging is very important in this area and hence we can test our approach on this problem.

When satellite imaging is used, we a huge amount of data is generated. But, a large portion of data is not informative because the huge portion of images contain only surface of ocean with no important object of interest or potentially land areas adjacent to sea. In order to make the monitoring process efficient, classic image processing techniques are used to determine regions of interest in aerial SAR images. A region of interest is a limited surface area, where existence of a ship is probable. First, land areas are removed and then ships, ship-like, and ocean regions are identified and then extracted as square image patches. These image patches are then fed into a classification algorithm to determine whether the region corresponds to a ship or not. If a ship detected with suspicious movement activity, then regulations can be enforced.

The dataset that we have used in our experiments is obtained from aerial SAR images of the South African Exclusive Economic Zone. The dataset is preprocessed into 51×51 pixels sub-images [6]. We define a binary classification problem, where each image instance is either contains ships (positive data points), or no-ship (negative data points). The dataset contains 1436 positive examples and 1436 negative sub-images. The labels are provided by experts. We recast the problem as a few-shot learning problem by assuming that only few of the data points are labeled. To solve this problem using knowledge transfer within our framework, we use the “EO Ships in Satellite Imagery" dataset [33]. The dataset is prepared to automate monitoring port activity levels and

 doi:10.20944/preprints201905.0030.v1

supply chain analysis and contains EO images extracted from Planet satellite imagery over the San Francisco Bay area with 4000 RGB 80×80 images. Again, each instance is either a ship image (a positive data point), or no-ship (a negative data point). The dataset is split evenly into positive and negative samples. Instances from both datasets are visualized in Figure 1 (left).

6.2. Methodology

We consider a deep CNNs with 2 layers of convolutional 3×3 filters as SAR encoder. We use N_F and $2N_F$ filters in these layers respectively, where N_F is parameter to be determined. We have used both maxpool and batch normalization layers in these convolutional layers. These layers are used as the SAR encoder sub-network in our framework, ϕ. We have used a similar structure for EO domain encoder, ψ, with the exception of using a CNN with three convolutional layers. The reason is that the EO dataset seems to have more details and more complex model can learn information content better. The third convolutional layer has $2N_F$ filters as well. The convolutional layers are followed by a flattening layer and a subsequent shared dense layer as the embedding space with dimension f which can be tuned as a parameter. After the embedding space layer, we have used a shallow two-layer classifier based on Eq. (3). We used TensorFlow for implementation and the Adam optimizer [34].

For comparison purpose, we compared our results against the following learning settings:

1) Supervised training on the SAR domain (ST): we just trained a network directly in the SAR domain using the few labeled SAR data points to generate a lower-bound for approach to demonstrate that knowledge transfer is effective. This approach is also a lower-bound because unlabeled SAR data points and their information content are discarded.

2) Direct transfer (DT): we just directly used the network that is trained on EO data directly in the SAR domain. In order to do this end, we resized the EO domain to 51×51 pixels so we can use the same shared encoder networks for both domains. As a result, potentially helpful details may be lost. This can be served as a second lower-bound to demonstrate that we can benefit from unlabeled SAR data.

3) Fine tuning (FT): we used the no transfer network from previous method, and fine-tuned the network using the few available SAR data points. As discussed before in the “Related Work" section, this is the main strategy that several prior works have used in the literature to transfer knowledge from the EO to the SAR domain and is served to compare against previous methods that use knowledge transfer.

In our experiments, we used a 90/10 % random split for training the model and testing performance. For each experiment, we report the performance on the SAR testing split to compare the methods. We use the classification accuracy rate to measure performance and whenever necessary and we used cross validation to tune the hyper parameters. We have repeated each experiment 20 times and have reported the average and the standard error bound to demonstrate statistical significance in the experiments.

In order to find the optimal parameters for the network structure, we used cross validation. We first preformed a set of experiments to empirically study the effect of dimension size (f) of the embedding space on performance of our algorithm. Figure 2a presents performance on SAR testing set versus dimension of the embedding space when 10 SAR labeled data per class is used for training. The solid line denotes the average performance over ten trials and the shaded region denotes the standard error deviation. We observe that the performance is quite stable when the embedding space dimension changes. This result suggests that because convolutional layers are served to reduce the dimension of input data, if the learned embedding space is discriminative for the source domain, then our method can successfully match the target domain distribution to the source distribution in the embedding. We conclude that for computational efficiency, it is better to select the embedding dimension to be as small as possible. We conclude from Figure 2a that increasing the dimension beyond 8 is not helpful. For this reason, we set the dimension of the embedding to be 8 for the rest our experiments in this paper. We performed a similar experiment to investigate the effect of number of filters N_F on performance. Figure 2b presents performance on SAR testing set versus this parameter. We conclude from Figure 2b that $N_F = 16$ is a good choice as using more filters in not helpful. We did not used a less value for N_F to avoid overfitting when the number of labeled data is less than 10.

Preprints (www.preprints.org) | NOT PEER-REVIEWED | Posted: 6 May 2019 doi:10.20944/preprints201905.0030.v1

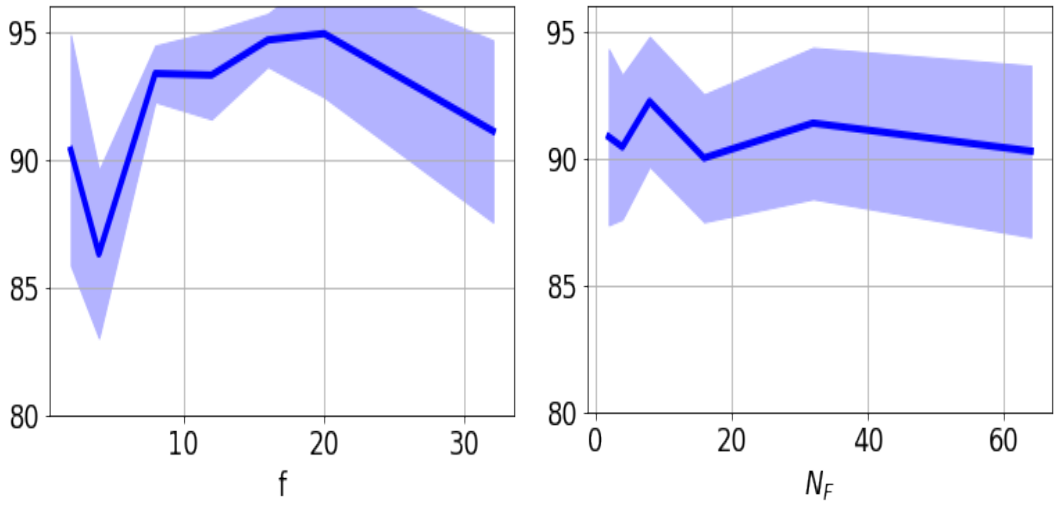

(a) Performance vs Embedding Dimension **(b)** Performance vs Number of Filters

Figure 2. The SAR test performance versus the dimension of the embedding space and the number of filters.

O	1	2	3	4	5	6	7
ST	58.5	74.0	79.2	84.1	85.2	84.9	87.2
FT	75.5	75.6	73.5	85.5	87.6	84.2	88.5
DT	71.5	67.6	71.4	68.5	71.4	71.0	73.1
FCS	86.3	86.3	82.8	94.2	87.8	96.0	91.1

Table 1. Comparison results for the SAR test performance.

6.3. Results

Figure 3 presents the performance results on the data test split for our method along with the three mentioned methods above, versus the number of labeled data points per class that has been used for the SAR domain. For each curve, the solid line denotes the average performance over all ten trials and the shaded region denotes the standard error deviation. These results accord with intuition. It can be seen that direct transfer is the least effective method as it uses no information from the second domain. Supervised training on the SAR domain is not effective in few shot learning regime, i.e. its performance is close to chance. Direct transfer method boosts the performance of supervised training in one-shot regime but after 2-3 labeled samples per class, as expected supervised training overtakes direct transfer. This is the consequence of using more target task data. In other words, direct transfer only helps to test the network on a better initial point compared to random initialization. Fine tuning can improve the direct performance, but only few-shot regime, and beyond few-shot learning regime the performance is similar to supervised training. In comparison, our method outperforms these methods as we have benefited from SAR unlabeled data points. For a more clear quantitative comparison, we have presented data in Figure 3 in Table 1 for different number of labeled SAR data points per class (O). It is also important to note that in the presence of enough labeled data in the target domain, supervised training would outperform our method because the netowkr is trained using solely the target domain data.

For having better intuition, Figure 4 denotes the Umap visualization [35] of the EO and SAR data points in the learned embedding as the output of the feature extractor encoders. Each points denotes on data point in the embedding which has been mapped to 2D plane for visualization. In this figure, we have used 5 labeled data points per class in the SAR domain. In Figure 4, each color corresponds to one of the classes. In Figures 4a and 4b, we have used real labels for visualization, and in Figures 4c and 4d, we have used the predicted labels by networks trained using our method for visualization. In Figure 4, the points with brighter red and darker blue colors are the SAR labeled data points that has been used in training. By comparing the top row with the bottom row, we see that the embedding is discriminative for both domains. Additionally, by comparing the left column with the right column, we see that the domain distributions are matched in the embedding class

Preprints (www.preprints.org) | NOT PEER-REVIEWED | Posted: 6 May 2019 doi:10.20944/preprints201905.0030.v1

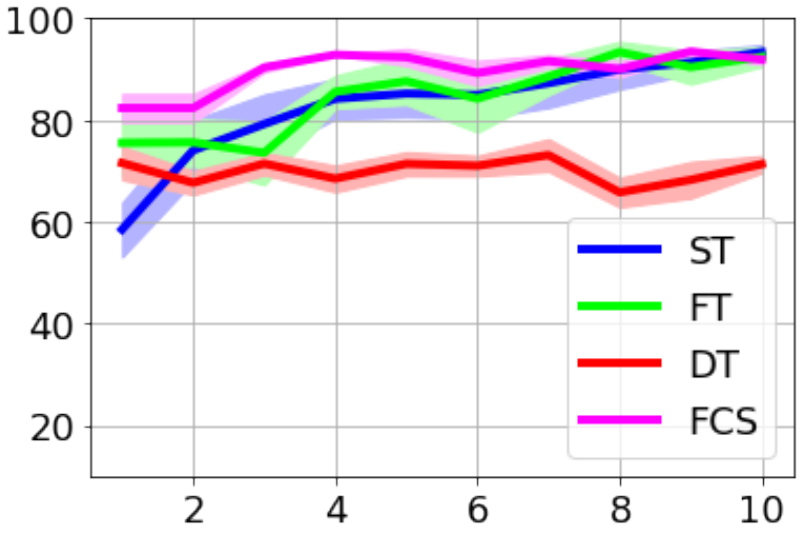

Figure 3. The SAR test performance versus the number of labeled data per class.

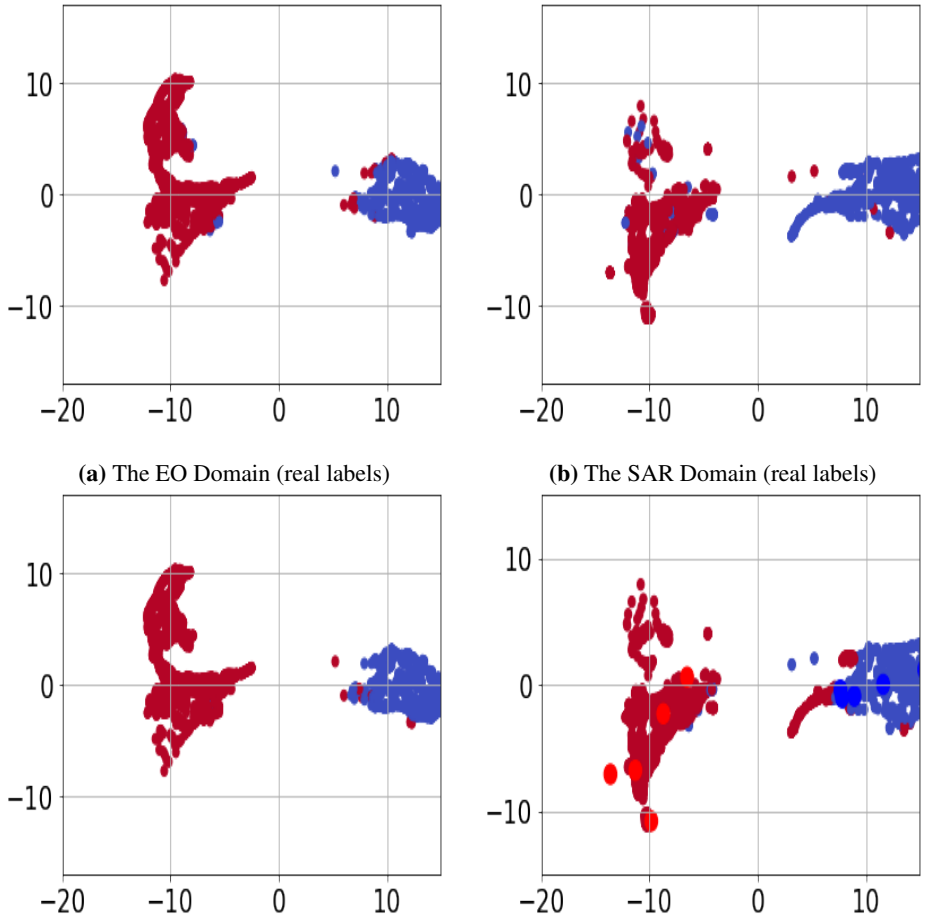

(a) The EO Domain (real labels)

(b) The SAR Domain (real labels)

(c) The EO Domain (predicted labels)

(d) The SAR Domain (labeled and unlabeled data)

Figure 4. Umap visualization of the EO versus the SAR dataset in the shared embedding space. (view in color.)

conditionally, suggesting our framework formulated is Eq. (3) is effective. This result suggests that learning an invariant embedding space can be served as a helpful strategy for transferring knowledge. Additionally, we see that labeled data points are important to determine the boundary between two classes which suggests that why

Preprints (www.preprints.org) | NOT PEER-REVIEWED | Posted: 6 May 2019 doi:10.20944/preprints201905.0030.v1

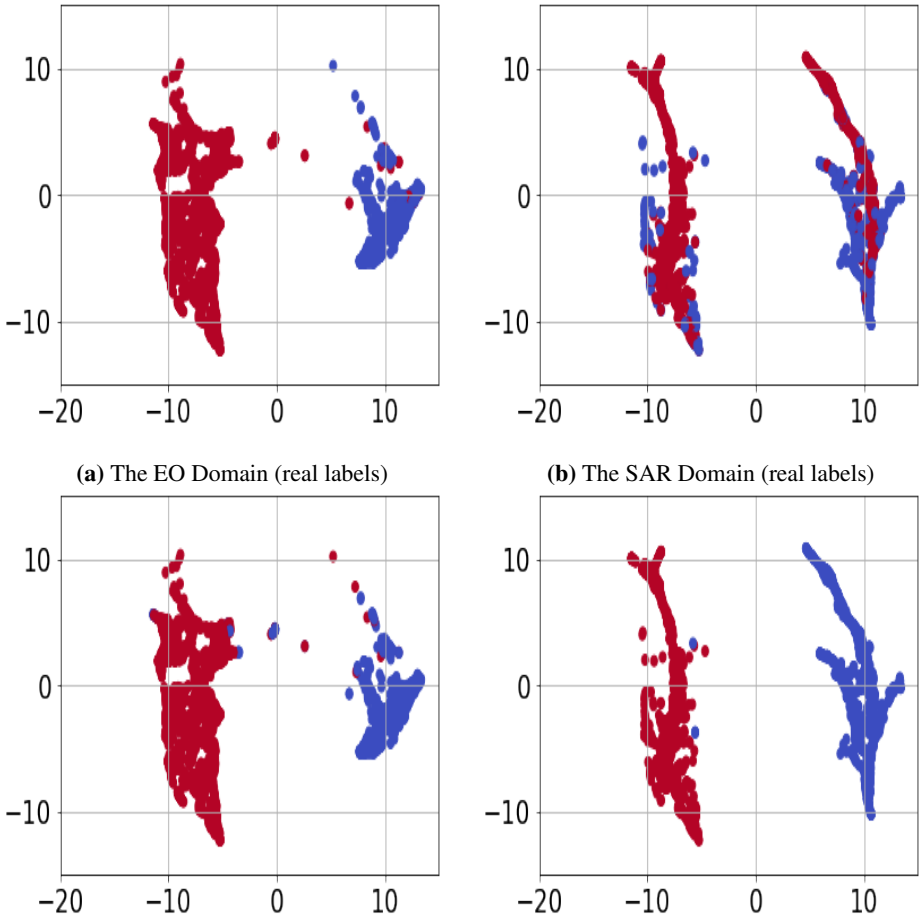

(a) The EO Domain (real labels)

(b) The SAR Domain (real labels)

(c) The EO Domain (predicted labels)

(d) The SAR Domain (predicted labels)

Figure 5. Umap visualization of the EO versus the SAR dataset for ablation study. (view in color.)

part of one of the classes (blue) is predicted mistakenly. This observation suggests that the boundary between classes depends on the labeled target data as the network is certain about labels of these data points.

We also performed an experiment to serve as an ablation study for our framework. Our previous experiments demonstrate that the first three terms in Eq. (3) are all important for successful knowledge transfer. We explained that the fourth term is important for class-conditional alignment. We solved Eq. (3) without considering the fourth term to study its effect. We have presented the Umap visualization of the datasets in the embedding space for a particular experiment in Figure 5. We observe that as expected the embedding is discriminative for EO dataset and predicted labels are close to the real data labels as the classes are separable. However, despite following a similar marginal distribution in the embedding space, the formed SAR clusters are not class-specific. We can see that in each cluster, we have data points from both classes and as a result the SAR classification rate is poor. This result demonstrates that all the terms in Eq. (3) are important for the success of our algorithm. We highlight that Figure 5 visualizes results of a particular experiments and we observed in some experiments the classes were matched, even when no labeled target data was used. However, this observations shows that the method is not stable. Using the few-labeled data helps to stabilize the algorithm.

7. Conclusions

In this paper, we addressed the problem of SAR image classification when only few labeled data are available. We formulated this problem as a semi-supervised domain adaption problem. Our idea is based on transferring knowledge from a related electro-optical domain problem where it is easy to generate labeled data. Our classification models are two deep convolutional neural networks that share their fully connected layers.

 doi:10.20944/preprints201905.0030.v1

The networks are trained such that the convolutional layers are served as two deep encoders that match the distributions of the two EO and SAR domains in an embedding space which is modeled as their shared output space. We provided theoretical analysis to explain why our algorithm minimizes an upperbound for target real risk and demonstrated effectiveness and applicability of our approach for the problem of ship classification in the area of maritime domain awareness. Despite being effective, a major restriction of our method is full overlap between the existing classes across the EO and the SAR domain. A future research direction is to remove this restriction by training the networks such that only the shared classes are matched in the embedding space.

1. Koo, V.; Chan, Y.; Vetharatnam, G.; Chua, M.Y.; Lim, C.; Lim, C.; Thum, C.; Lim, T.; bin Ahmad, Z.; Mahmood, K.; others. A new unmanned aerial vehicle synthetic aperture radar for environmental monitoring. *Progress In Electromagnetics Research* **2012**, *122*, 245–268.
2. Maitre, H. *Processing of Synthetic Aperture Radar (SAR) Images*; Wiley, 2010.
3. Deng, J.; Dong, W.; Socher, R.; Li, L.J.; Li, K.; Fei-Fei, L. Imagenet: A large-scale hierarchical image database. 2009 IEEE conference on computer vision and pattern recognition. Ieee, 2009, pp. 248–255.
4. Rostami, M.; Huber, D.; Lu, T.C. A crowdsourcing triage algorithm for geopolitical event forecasting. Proceedings of the 12th ACM Conference on Recommender Systems. ACM, 2018, pp. 377–381.
5. Malmgren-Hansen, D.; Kusk, A.; Dall, J.; Nielsen, A.; Engholm, R.; Skriver, H. Improving SAR automatic target recognition models with transfer learning from simulated data. *IEEE Geoscience and Remote Sensing Letters* **2017**, *14*, 1484–1488.
6. Schwegmann, C.; Kleynhans, W.; Salmon, B.; Mdakane, L.; Meyer, R. Very deep learning for ship discrimination in synthetic aperture radar imagery. IEEE International Geo. and Remote Sensing Symposium, 2016, pp. 104–107.
7. Huang, Z.; Pan, Z.; Lei, B. Transfer learning with deep convolutional neural network for SAR target classification with limited labeled data. *Remote Sensing* **2017**, *9*, 907.
8. Chen, S.; Wang, H.; Xu, F.; Jin, Y. Target classification using the deep convolutional networks for SAR images. *IEEE Trans. on Geo. and Remote Sens.* **2016**, *54*, 4806–4817.
9. Shang, R.; Wang, J.; Jiao, L.; Stolkin, R.; Hou, B.; Li, Y. SAR Targets Classification Based on Deep Memory Convolution Neural Networks and Transfer Parameters. *IEEE Journal of Selected Topics in Applied Earth Observations and Remote Sensing* **2018**, *11*, 2834–2846.
10. Pan, S.; Yang, Q. A survey on transfer learning. *IEEE Transactions on knowledge and data engineering* **2010**, *22*, 1345–1359.
11. Zhang, D., J.; Heng, W.; Ren, K.; Song, J. Transfer Learning with Convolutional Neural Networks for SAR Ship Recognition. IOP Conference Series: Materials Science and Engineering. IOP Publishing, 2018, Vol. 322, p. 072001.
12. Wang, Z.; Du, L.; Mao, J.; Liu, B.; Yang, D. SAR Target Detection Based on SSD With Data Augmentation and Transfer Learning. *IEEE Geoscience and Remote Sensing Letters* **2018**.
13. Lang, H.; Wu, S.; Xu, Y. Ship classification in SAR images improved by AIS knowledge transfer. *IEEE Geoscience and Remote Sensing Letters* **2018**, *15*, 439–443.
14. Motiian, S.; Jones, Q.; Iranmanesh, S.; Doretto, G. Few-shot adversarial domain adaptation. Advances in Neural Information Processing Systems, 2017, pp. 6670–6680.
15. Redko, I.and Habrard, A.; Sebban, M. Theoretical analysis of domain adaptation with optimal transport. Joint European Conference on Machine Learning and Knowledge Discovery in Databases. Springer, 2017, pp. 737–753.
16. Villani, C. *Optimal transport: old and new*; Vol. 338, Springer Science & Business Media, 2008.
17. Gretton, A.; Smola, A.; Huang, J.; Schmittfull, M.; Borgwardt, K.; Schölkopf, B. Covariate shift by kernel mean matching. *Dataset shift in machine learning* **2009**.
18. Rabin, J.; Peyré, G.; Delon, J.; Bernot, M. Wasserstein barycenter and its application to texture mixing. International Conference on Scale Space and Variational Methods in Computer Vision. Springer, 2011, pp. 435–446.
19. Kolouri, S.; Rohde, G.K.; Hoffman, H. Sliced Wasserstein Distance for Learning Gaussian Mixture Models. IEEE Conference on Computer Vision and Pattern Recognition, 2018, pp. 3427–.
20. Kodirov, E.; Xiang, T.; Fu, Z.; Gong, S. Unsupervised domain adaptation for zero-shot learning. Proceedings of the IEEE International Conference on Computer Vision, 2015, pp. 2452–2460.
21. Goodfellow, I.; Pouget-Abadie, J.; Mirza, M.; Xu, B.; Warde-Farley, D.; Ozair, S.; Courville, A.; Bengio, Y. Generative adversarial nets. Advances in neural information processing systems, 2014, pp. 2672–2680.

22. Courty, N.; Flamary, R.; Tuia, D.; Rakotomamonjy, A. Optimal transport for domain adaptation. *IEEE TPAMI* **2017**, *39*, 1853–1865.
23. Daume III, H.; Marcu, D. Domain adaptation for statistical classifiers. *Journal of artificial Intelligence research* **2006**, *26*, 101–126.
24. Kolouri, S.; Pope, P.E.; Martin, C.E.; Rohde, G.K. Sliced-Wasserstein Auto-Encoders. *International Conference on Learning Representation (ICLR)* **2019**.
25. Bonneel, N.; Rabin, J.; Peyré, G.; Pfister, H. Sliced and Radon Wasserstein barycenters of measures. *Journal of Mathematical Imaging and Vision* **2015**, *51*, 22–45.
26. Carriere, M.; Cuturi, M.; Oudot, S. Sliced wasserstein kernel for persistence diagrams. *arXiv preprint arXiv:1706.03358* **2017**.
27. Long, M.; Wang, J.; Ding, G.; Sun, J.; Yu, P.S. Transfer joint matching for unsupervised domain adaptation. Proceedings of the IEEE conference on computer vision and pattern recognition, 2014, pp. 1410–1417.
28. Damodaran, B.; Kellenberger, B.; Flamary, R.; Tuia, D.; Courty, N. DeepJDOT: Deep Joint distribution optimal transport for unsupervised domain adaptation. *arXiv preprint arXiv:1803.10081* **2018**.
29. Kolouri, S.; Park, S.R.; Thorpe, M.; Slepcev, D.; Rohde, G.K. Optimal Mass Transport: Signal processing and machine-learning applications. *IEEE Signal Processing Magazine* **2017**, *34*, 43–59.
30. Rabin, J.; Peyré, G.; Delon, J.; Bernot, M. Wasserstein barycenter and its application to texture mixing. International Conference on Scale Space and Variational Methods in Computer Vision. Springer, 2011, pp. 435–446.
31. Bonnotte, N. Unidimensional and evolution methods for optimal transportation. PhD thesis, Paris 11, 2013.
32. Santambrogio, F. Optimal transport for applied mathematicians. *Birkäuser, NY* **2015**, pp. 99–102.
33. Hammell, R. Ships in Satellite Imagery, 2017. data retrieved from Kaggle, https://www.kaggle.com/rhammell/ships-in-satellite-imagery.
34. Kingma, D.P.; Ba, J. Adam: A method for stochastic optimization. *arXiv preprint arXiv:1412.6980* **2014**.
35. McInnes, L.; Healy, J.; Melville, J. Umap: Uniform manifold approximation and projection for dimension reduction. *arXiv preprint arXiv:1802.03426* **2018**.